On the Supersonic Flame Structure in the HyShot II Scramjet Combustor

Christer Fureby
The Swedish Defence Research Organization
SE 147 25 Tumba, Stockholm, Sweden

1 Introduction and Background

Understanding of the multi-disciplinary physical processes in the flow-path of a scramjet engine is crucial for the enabling of this technology, considered the most promising for hypersonic flight. The flow in such engines remains supersonic throughout, preventing the pressure losses and structural challenges involved in decelerating the flow to subsonic speeds. However, this necessitates that the mixing and combustion processes in the engine occur within supersonic flow, with residence times of O(1) ms. Within this short time interval, the fuel and air must mix, ignite and combust prior to discharging through the nozzle. Laboratory, ground testing and flight-testing experiments, together with high-fidelity numerical simulations, comprise the tools available to fill the gap in scramjet combustor knowledge. In this study, we combine results from high-fidelity Large Eddy Simulation (LES), using finite-rate chemistry models and skeletal reaction mechanisms, with experimental pressure data and visualization of the shock-train and the heat-release to elucidate the key features of the flow of the HyShot II combustor. We specifically focus on the conditions of experiments performed in the High Enthalpy Shock Tunnel Göttingen (HEG), emulating flight conditions at 27 km altitudes, [1]. The flame structure is characterized using an extended Williams diagram.

2 Large Eddy Simulation Models for Supersonic Combustion

The Large Eddy Simulation (LES) model employed is based on a reacting-flow model in which the mixture is assumed to be a linear viscous fluid with Fourier heat conduction and Fickian diffusion. The viscosity is calculated using Sutherland's law while the thermal conductivity and species diffusivities are computed from the viscosity using constant Prandtl and species Schmidt numbers. The mixture thermal and caloric equations-of-state are obtained assuming that each species is a thermally perfect gas. The combustion model is based on finite-rate Arrhenius reaction rates.

The LES model use implicitly-filtered mass, momentum, energy and species equations, [2], in which the subgrid stress tensor and flux vectors are closed by the mixed model, [3]. The filtered reaction-

Correspondence to: fureby@foi.se

rate terms are modeled with the Partially Stirred Reactor (PaSR) model, [4-5], which is a multi-scale model based on the observation, [6], that combustion often takes place in dispersed fine-structure regions surrounded by low chemical activity. Here, the filtered reaction rates are approximated as a weighted average of the fine-structure and surrounding reaction rates using the reacting volume fraction, γ^*, as the weighting function. Subgrid mass and energy equations are solved in all LES cells for both fine-structure and surrounding mass-fractions and temperature, using the fine-structure residence time, τ^*. Here, τ^* and γ^* are modeled using the Kolmogorov, and global chemical time-scales, [4]. The LES-PaSR model has been widely used, and is validated for laboratory combustors, [7-8], afterburners, [9], gas turbines, [10], and scramjets, [11].

The LES equations are solved using a fully-explicit, density-based, compressible finite-volume code based on the OpenFOAM library, [12]. High-order monotonicity-preserving reconstruction of the convective fluxes and central differencing of the diffusive fluxes, [13], is combined with a total variation diminishing based Runge-Kutta time integration scheme to result in a second-order accurate algorithm with a Courant number limitation of ~0.2. The chemical source terms are evaluated using an operator-splitting approach together with a stiff Rosenbrock solver, [14].

We use the skeletal 7-step Davidenko *et al.* (D7) reaction mechanism, [15], which compare favorably with comprehensive mechanisms, e.g. [16], with respect to the adiabatic flame temperature, T_{ad}, ignition delay time, τ_{ign}, extinction strain rate, σ_{ext}, and laminar flame speed, s_u. Sensitivity analysis reveals that both s_u and σ_{ext} are sensitive primarily to the chain-branching reactions $H_2+O \Leftrightarrow OH+H$ and $H+O_2 \Leftrightarrow OH+O$ and the initiation step $H_2+O_2 \Leftrightarrow OH+OH$. D7 captures this sensitivity well, and is capable of representing the explosion limits of H_2-air mixtures.

3 LES of the HyShot II Combustor

The combustor considered is the HyShot II combustor, [1], experimentally studied in the HEG shock tunnel. The flow-path of the HyShot II HEG shock tunnel model duplicates the flight configuration, [17] and consists of an intake ramp, a rectilinear combustor, and a single-sided exhaust nozzle. Here, we focus on the HEG combustor section, shown in figure 2, from test condition XIII, [1], representing flight conditions at 28 km altitude. The combustor has a cross-section of 9.8×75.0 mm^2 and a length of 0.3 m, after which a one-sided diverging-area nozzle is mounted. Gaseous H_2 is injected orthogonal to the air-stream, having an average velocity of 1720 m/s, a temperature of 1350 K and a pressure of 127 kPa, resulting in an equivalence ratio of $\phi \approx 0.28$, through four ϕ2.0 mm porthole Ma 1.0 injectors 58 mm downstream of the combustor leading edge. The experimental data include Schlieren and OH* chemiluminescence, body and cowl wall pressure data, and body heat-flux data, [1]. A grid of ~100 million cells is used with clustering at the combustor walls. Dirichlet boundary conditions are used for all variables at the inlet, with profiles obtained from RANS, and at the H_2 injectors. At the outlet, all variables are extrapolated. At the combustor walls, a no-slip LES wall-model is used together with zero Neumann conditions for all other variables.

Figure 2 present a composite figure of the reacting flow in the HyShot II combustor. The two large figures, showing the full combustor, describe the flow in terms of an iso-surface of the second invariant of the velocity gradient tensor, λ_2, colored by the axial velocity, v_x, and the mixing and reaction processes in terms of volumetric renderings of the temperature, T, and the H_2O, OH and H_2 mass fractions, Y_{H2O}, Y_{OH}, Y_{H2}, respectively. The three small figures, showing a small volume around one of the central injectors, show an iso-surface of λ_2, colored by v_x, and superimposed volumetric renderings of H_2O, OH and H_2 mass fractions, and of the pressure gradient, ∇p, and the chemical explosive mode eigenvalue, λ_e, [18], describing the shock-train and the reactive state of the mixture.

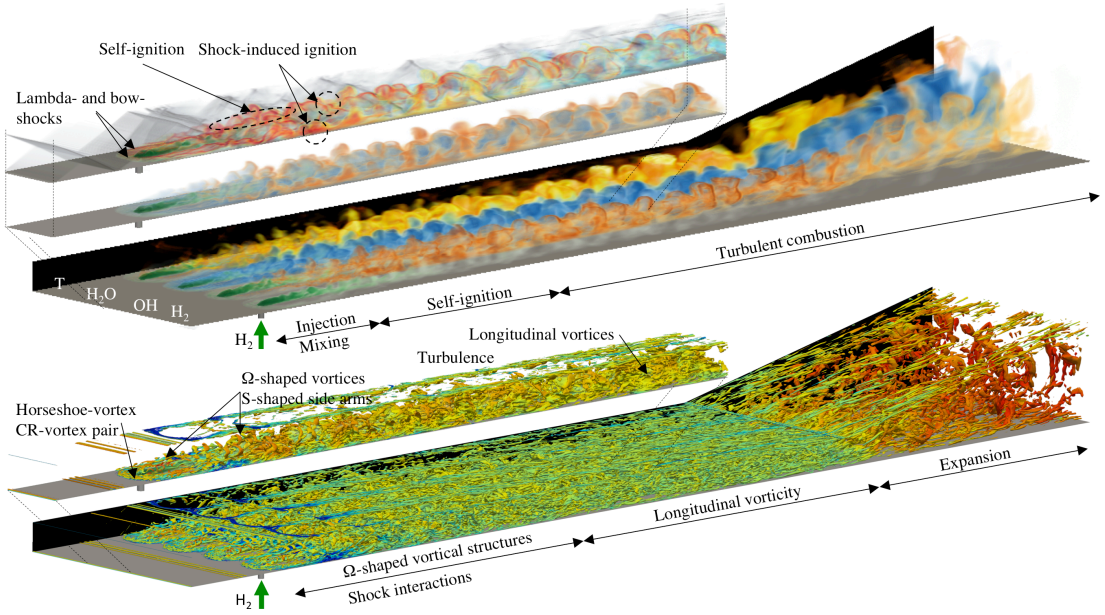

Figure 1. Reacting flow in the HyShot II combustor in terms of volumetric renderings of the pressure gradient, ∇p, chemical explosive mode eigenvalue, λ_e, temperature, T, H_2O, OH and H_2 mass fractions and iso-surfaces of the second invariant of the velocity gradient tensor, λ_2, colored by the axial velocity, v_x.

The flow can broadly be divided into an injection and mixing region, a self-ignition region, and a fully developed turbulent combustion region. The flow is governed by (i) four horseshoe vortex systems wrapping around the H_2-jets, developing in front of each injector as a result of the flow stagnation and boundary-layer separation, the latter resulting in a lambda-shock ahead of the bow-shock; (ii) Four counter-rotating vortex pairs along the average trajectory of each H_2-plume, starting at the leading edges of the jet shear-layers; (iii) Jet shear-layer vortices wrapping around the jets, and developing due to Kelvin-Helmholtz instabilities in the jet-shear layers. Close behind the injectors, these flow structures often appear as incoherent S-shaped side vortex arms, spanwise vortex rollers and small standing vortices, which further downstream combine into Ω-shaped vortex loops that gradually develops (by vortex-vortex interactions) into longitudinal vortices,

A small amount of H_2 is peeled-off the jets as they discharge into the combustor, and rapidly mixed with the air by the jet shear-layer vortices, and ignited by the temperature increase due to the lambda- and bow-shocks. This results in radicals (e.g. O, H, OH), and H_2O, forming a thin sheet over each H_2 plume being advected downstream. Along the self-ignition region, the vortex loops gradually becomes more regularly spaced, whilst providing the mixing of hot air, H_2, radicals and H_2O resulting in self-ignition of the H_2-plumes, facilitated by the shock-plume interactions. Some H_2 is drawn into the horseshoe vortex systems where it gradually becomes heated and mixed with the hot air and radicals. When these structures are impinged on by the reflected shocks, ignition occurs. Neighboring horseshoe vortex system legs combine, forming small Ω-shaped vortex loops between the primary H_2 plumes. Further downstream, the vortical structures gradually lose their coherence and develop longitudinal vortices, and radicals and product species occur intermittently.

The species (H_2, OH and H_2O) distributions show a rather entwined and complex behavior, typically, with OH, O and H occurring between H_2, air and H_2O. The radicals O and H occur in thin, wrinkled,

layers fragmented by the turbulence, whereas OH shows super-equilibrium levels along the reaction fronts and equilibrium levels on the product side. Large-scale turbulence creates large scale wrinkling and small-scale turbulence creates small scale wrinkling of the species distributions. Pockets of radicals (O, H and OH) can be observed to form in regions in which shock-shock, shock-boundary layer and particularly shock-plume interactions takes place.

The chemical explosive mode eigenvalue, λ_e, show positive values (red), representative of mixtures prone to ignite and burn, in the horseshoe vortex legs, along the outer edges of the S- and Ω-shaped plume vortices, and in spots just downstream of where a reflected shock has impinged on a H_2 containing mixture state. λ_e show negative values (blue), representative of reactive but non-explosive, or burned mixtures, in the middle and downstream part of the plume. The negative regions of λ_e widen with downstream distance from the injectors as most of the fuel is consumed.

Figures 2a and 2b compare longitudinal profiles of the time-averaged body-side and cowl-side wall-pressures, ⟨p⟩, and the body-side heat-flux, ⟨h⟩, between experimental data, [1], and RANS, [1], and LES predictions. Good agreement between LES and RANS and the experimental data is observed for ⟨p⟩, which shows a linear increase along the combustor with a superimposed shock-train developing from the combustor leading edge. For ⟨h⟩ the LES predictions agree significantly better with the experimental data than the RANS predictions. The differences between the LES and RANS are mainly due to the higher spatial resolution and the resolved large-scale unsteadiness.

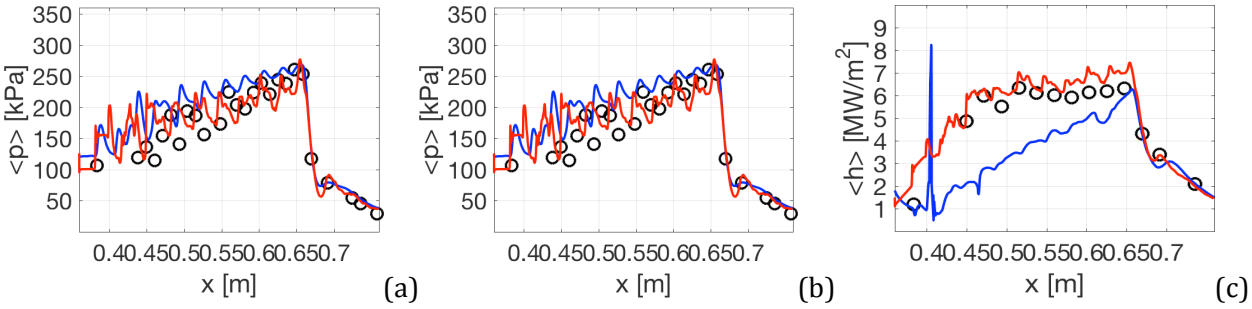

Figure 2. Predicted (lines) and measured, [1], (circles) (a) body wall pressure, (b) cowl wall pressure and (c) body heat flux from (—) RANS, [1], and from (—) LES.

From the computational density gradient and experimental Schlieren images, [19], in figure 3a the shock-train and plume are observed to be in acceptable agreement. The plume is somewhat more apparent in the LES than in the Schlieren images, which may be due to the absence of the smallest scales in the LES. The computational heat-release agrees well in topology with the plume topology in both the experimental Schlieren images and in the LES.

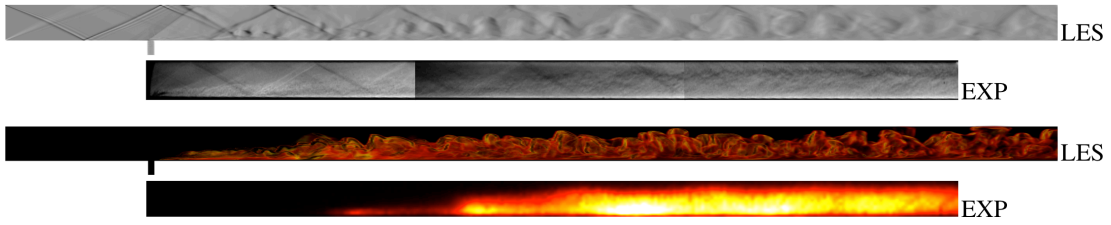

Figure 3. Computational and experimental Schlieren images, [19], in gray scale (top) together with computational heat-release and experimental OH chemiluminescence (bottom).

4 Supersonic Flame Structures

The mixing and flame topology is very complicated as observed in figure 1, and in order to simplify it's interpretation we present in figure 4a a 3D scatter plots of the temperature, T, mixture fraction, z, and coordinate, x, along the combustor axis, colored by the chemical explosive mode eigenvalue, λ_e, [18]. The projection on the T-z plane reveals a diffusion flame structure, with a peak in T close to z_{st}, but with a large variation in T, reminiscent of local extinction. The highest values of λ_e occur close to z_{st}, but on the O_2 side, and the shock-train is visible as variations in T along the x-axis. The branch starting at z=1 (at x=0.42) represents the H_2 rich mixture from the injectors and is physically associated with the main plumes and the horseshoe vortex systems, along which both T and λ_e increase with downstream distance. This branch merges with the air branch from the inlet (at x=0.34) along which λ_e is negative as it consists of a non-reactive mixture. When these branches merge λ_e increase at first as the mixture becomes explosive (due to the H_2-O_2 mixing at high T), to then gradually decrease to negative values, representing combustion products (H_2O). Some of inflow air pass through the combustor without participating in the reactions (blue). The mixture temperature decrease along the nozzle as the flow accelerates and thrust is generated.

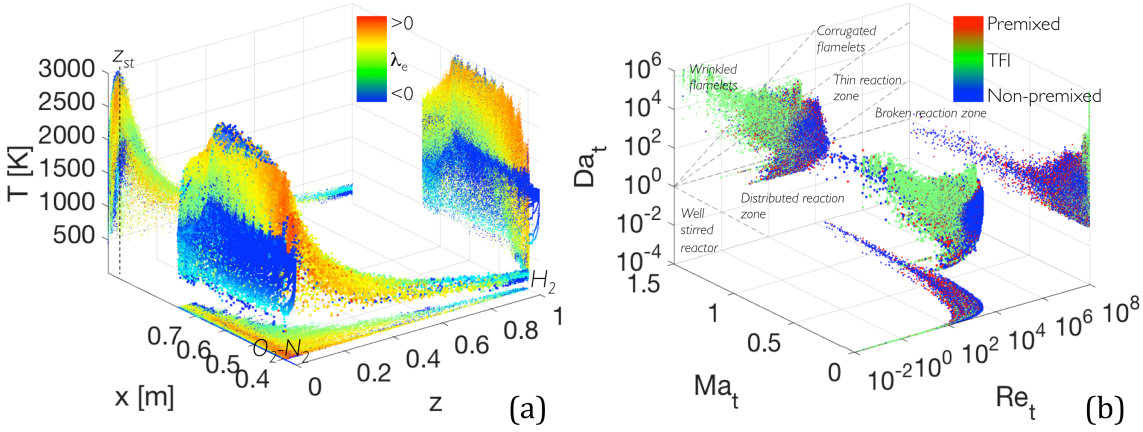

Figure 4. (a) 3D scatter plots of the temperature, T, mixture fraction, z, and coordinate, x, along the combustor axis, colored by the chemical explosive mode eigenvalue, λ_e, and (b) 3D scatter plot of the turbulent Damköhler number, Da_t, Reynolds number, Re_t, and Mach number, Ma_t, colored by the heat-release indexed Takeno flame index.

In figure 4b we present a 3D scatter plot of the turbulent Damköhler number, Da_t, Reynolds number, Re_t, and Mach number, Ma_t, (based on the velocity fluctuations) colored by the heat-release indexed Takeno flame index. This figure corresponding to an extended version of the Williams diagram, [20], and shows that scramjet combustion typically occurs in the region $10^2<Re_t<10^4$ and $10^{-1}<Da_t<10^2$, as suggested by Williams, [20], but also that significant compressible effects occurs as evident by the surprisingly high Ma_t numbers observed. Regions of high Ma_t ($Ma_t>0.75$) occur in the counter-rotating vortex pairs, in regions of shock-reflections, and in regions where shock-induced ignition occurs, i.e. in localized regions along the horseshoe vortex legs and in spots on the plume edges in which the reflected shocks impinges on a heated mixture of H_2, O_2 and radicals. The high Ma_t-number state is primarily of non-premixed nature (blue) but with some premixed elements embedded. The detailed flame structure in scramjet combustion is not very well known, and it would be appropriate to try and characterize this using Direct Numerical Simulations.

5 Discussion

High-fidelity LES predictions of the HyShot II combustor are presented and compared against experimental data and RANS predictions. Good agreement is generally observed, indicating that the LES captures the essential physics. The LES results are then used to elucidate the flow and flame physics with the intent of providing improved understanding of the interacting self-ignition and flame-stabilization mechanisms. In particular it is observed that the flame typically reside in the region $10^2<Re_t<10^4$ and $10^{-1}<Da_t<10^2$, and experience significant turbulent Ma numbers, which may have an effect on the turbulent flame structure. The observation that the most probable flame regime spans several zones suggest that methods capable of handling various, *a priori* unknown, flame topologies, such as finite rate chemistry LES methods should be employed in simulations.

References

[1] Schramm J.M., Karl S., Hannemann K & Streelant J.; 2008, "Ground Testing of the HyShot II Scramjet Configuration in HEG", AIAA 2008-2547.
[2] Menon S. & Fureby C.; 2010, "Computational Combustion", In Encyclopedia of Aerospace Engineering, Eds. Blockley R. & Shyy W., John Wiley & Sons.
[3] Bensow R. & Fureby C.; 2007, "On the Justification and Extension of Mixed Models in LES", J. Turb. **8**, N54, p. 1.
[4] Sabelnikov V. & Fureby C.; 2013, "LES Combustion Modeling for High Re Flames using a Multi-Phase Analogy", Comb. Flame, **160**, p 83.
[5] Fureby C.; 2009, "LES Modeling of Combustion for Propulsion Applications". Phil. Trans. R. Soc. A, **367**, p 2957.
[6] Tanahashi M., Fujimura M. & Miyauchi T.; 2000, "Coherent Fine Scale Eddies in Turbulent Premixed Flames", Proc. Comb. Inst. **28**, p 5729.
[7] Nogenmyr K.J., Petersson P., Bai X.S., Fureby C., Collin R., Lantz A. Linne M. & Aldén M.; 2011, "Structure and Stabilization Mechanism of a Stratified Premixed Low Swirl Flame", Proc. Comb. Inst., **33**, p 1567
[8] Fedina E. & Fureby C.; 2011, "A Comparative Study of Flamelet and Finite Rate Chemistry LES of an Axisymmetrc Dump Combustor", J. Turb, **12**, N24.
[9] Fureby C.; 2017, "A Comparative Study of Large Eddy Simulation (LES) Combustion Models applied to the Volvo Validation Rig ", AIAA 2017-1575.
[10] Bulat G., Fedina E., Fureby C., Meier W. & Stopper U.; 2014, "Reacting Flow in an Industrial Gas Turbine Combustor: LES and Experimental Analysis", Proc. Comb. Inst., **35**, p 3175.
[11] Chapuis M., Fedina E. Fureby C., Hannemann K., Karl S. & Martinez Schramm J.; 2012, "A Computational Study of the HyShot II Combustor Performance", Proc. Comb. Inst., **34**, p 2101.
[12] Weller H.G., Tabor G., Jasak H. & Fureby C.; 1997, "A Tensorial Approach to CFD using Object Oriented Techniques", Comp. in Physics, **12**, p 629.
[13] Drikakis D., Fureby C., Grinstein F.F. & Liefendahl M.; 2007, "ILES with Limiting Algorithms", In Implicit Large Eddy Simulation: Computing Turbulent Fluid Dynamics, Eds. Grinstein F.F., Margolin L. & Rider B., CUP, p 94.
[14] Hairer E. & Wanner G.; 1991, "Solving Ordinary Differential Equations", II: Stiff and Differential-Algebraic Problems, 2nd Ed., Springer Verlag.
[15] Davidenko D.M., Gökalp I., Dufour E. & Magre P.; 2003, "Numerical Simulation of Hydrogen Supersonic Combustion and Validation of Computational Approach", AIAA 2003-7003.
[16] O'Conaire M., Curran H.J., Simmie J.M., Pitz W.J. & Westbrook C.K.; 2004, "A Comprehensive Modeling Study of Hydrogen Oxidation", Int. J. Chem. Kin., **36**, p 603.
[17] Hass N.E., Smart M.K. & Paull A.; 2005, "Flight Data Analysis of HyShot 2", AIAA 2005-3354.
[18] Lu T.F., Yoo C.S., Chen J.H. & Law C.K.; 2010, "Three-Dimensional Direct Numerical Simulation of a Turbulent Lifted Hydrogen Jet Flame in Heated Coflow: A Chemical Explosive Mode Analysis", J. Fluid Mech., **652**, p 45.
[19] Laurence S.J., Schramm J.M., Karl S. & Hannemann K; 2011, "An Experimental Investigation of Steady and Unsteady Combustion Phenomena in the HyShot II Combustor", AIAA 2011-2310.
[20] Balakrishnan G. & Williams F.A.; 1994, "Turbulent Combustion Regimes for Hypersonic Propulsion Employing Hydrogen-Air Diffusion Flames", J. Prop., **10**, p 434.